

# Delivering nanomedicine to solid tumors

Rakesh K. Jain and Triantafyllos Stylianopoulos

**Abstract** | Recent advances in nanotechnology have offered new hope for cancer detection, prevention, and treatment. While the enhanced permeability and retention effect has served as a key rationale for using nanoparticles to treat solid tumors, it does not enable uniform delivery of these particles to all regions of tumors in sufficient quantities. This heterogeneous distribution of therapeutics is a result of physiological barriers presented by the abnormal tumor vasculature and interstitial matrix. These barriers are likely to be responsible for the modest survival benefit offered by many FDA-approved nanotherapeutics and must be overcome for the promise of nanomedicine in patients to be realized. Here, we review these barriers to the delivery of cancer therapeutics and summarize strategies that have been developed to overcome these barriers. Finally, we discuss design considerations for optimizing the delivery of nanoparticles to tumors.

Jain, R. K. & Stylianopoulos, T. *Nat. Rev. Clin. Oncol.* 7, 653–664 (2010); published online 14 September 2010; doi:10.1038/nrclinonc.2010.139

## Introduction

Rapid advances in nanotechnology have permitted the incorporation of multiple therapeutic, sensing and targeting agents into nanoparticles (for example, liposomes, viruses and quantum dots), with a size range of 1–1,000 nm. These agents have offered new hope for detection, prevention, and treatment in oncology. Nanomedicine for cancer therapy is advantageous over conventional medicine because it has the potential to enable the preferential delivery of drugs to tumors owing to the enhanced permeability and retention (EPR) effect, and the delivery of more than one therapeutic agent for combination therapy. Other advantages of nanomedicine include specific binding of drugs to targets in cancer cells or the tumor microenvironment, simultaneous visualization of tumors using innovative imaging techniques, enhanced drug-circulation times, controlled drug-release kinetics, and superior dose scheduling for improved patient compliance.<sup>1–6</sup> Furthermore, many widely used conventional chemotherapeutics, such as taxanes, include synthetic solvents (for example, castor oil and polysorbate 80) that directly contribute to adverse effects.<sup>7–9</sup> Finally, many tumor types are inherently resistant to available chemotherapeutics. Nanomedicine has the potential to overcome these problems.<sup>10,11</sup>

Over 20 nanoparticle therapeutics have been approved by the FDA for clinical use.<sup>12,13</sup> Nanoparticle formulations for the treatment of solid tumors (Table 1) include liposomes (such as pegylated liposomal doxorubicin and liposomal daunorubicin), albumin-bound paclitaxel, polymeric particles (such as methoxy-PEG-poly[D,L-lactide] taxol) and many more formulations that are in preclinical

and/or clinical trials.<sup>12</sup> Although less toxic than conventional therapies, these agents are still associated with adverse effects, such as stomatitis and palmar–plantar erythrodysesthesia for pegylated liposomal doxorubicin<sup>14</sup> and sensory neuropathy and nausea for albumin-bound paclitaxel.<sup>7</sup> Moreover, these agents are expensive, and the increase in overall survival is modest in many cases (Table 1). Therefore, a better understanding of the barriers that prevent efficacy and uniform delivery of nanoparticles into tumors is needed to develop strategies to improve treatment.

Transport of a therapeutic agent from the systemic circulation to cancer cells is a three-step process. First, nanoparticles flow to different regions of tumors via blood vessels. They must then cross the vessel wall, and finally, penetrate through the interstitial space to reach the target cells. Delivery of diagnostic and therapeutic agents differs dramatically between tumor and normal tissues because of differences in their structure. The abnormal organization and structure of the tumor vasculature leads to tortuous and leaky vessels and heterogeneous blood flow.<sup>15,16</sup> In addition, the lack of functional lymphatic vessels and the vascular hyperpermeability inside tumors results in interstitial hypertension.<sup>17</sup> This uniformly elevated interstitial fluid pressure (IFP) reduces convective transport, while the dense extracellular matrix hinders diffusion.<sup>18</sup> In this Review, we discuss the barriers to nanomedicine delivery and present strategies to overcome them. Finally, we propose design considerations to optimize delivery of nanotherapeutics to solid tumors.

## Abnormal blood and lymphatic networks

Blood-flow rate and vascular morphology (that is, the geometric arrangement, diameter, length and number of blood vessels) affect the movement of compounds through the vasculature.<sup>19–22</sup> Blood vessels in tumors are highly irregular in their architecture compared with

Edwin L. Steele  
Laboratory, Department  
of Radiation Oncology,  
Massachusetts  
General Hospital and  
Harvard Medical  
School, 100 Blossom  
Street, Boston,  
MA 02114, USA  
(R. K. Jain,  
T. Stylianopoulos).

Correspondence to:  
R. K. Jain  
jain@  
stele.mgh.harvard.edu

## Competing interests

R. K. Jain declares associations with the following companies: Alnylam, Astellas, AstraZeneca, Dyax, Enlight Biosciences, Genzyme, Millenium, MorphoSys, Noxxon, Pfizer, Roche and SynDevRx. See the article online for full details of the relationships. T. Stylianopoulos declares no competing interests.

**Key points**

- Enhanced permeability and retention is the primary rationale for using nanoparticles in oncology; however, only a few nanotherapeutics have been approved for the treatment of solid tumors and the overall survival benefit from these is modest in many cases
- The abnormal structure of tumor vessels results in heterogeneous tumor perfusion and extravasation, and a hostile tumor microenvironment that fuels drug resistance and tumor progression
- In highly fibrotic or desmoplastic tumors, the extracellular matrix consisting of an interconnected network of collagen fibers blocks penetration of large nanoparticles leaving them concentrated in perivascular regions
- Normalization of the vascular network with antiangiogenic therapy and normalization of the extracellular matrix using matrix-modifying agents has the potential to improve the delivery and efficacy of nanomedicine
- Targeting nanoparticles to cancer cells or tumor-associated endothelial cells is another promising strategy but may be limited by spatial and temporal heterogeneity in the expression of the targets
- Development of nanoparticles that release therapeutic agents in response to the tumor microenvironment or an external stimulus (for example, light, ultrasound, heat, electric or magnetic fields) may also improve the delivery of nanomedicine

**Table 1** | Nanoparticle formulations for the treatment of solid tumors\*

Generic name	Trade name(s)	Indication	Benefit
Pegylated liposomal doxorubicin	Doxil® and Caelyx®	HIV-related Kaposi's sarcoma	No statistically significant change in overall survival (23 weeks) vs doxorubicin, bleomycin and vincristine treatment (22.3 weeks) for HIV-related Kaposi's sarcoma <sup>144</sup>
		Metastatic ovarian cancer	Statistically significant overall survival improvement (108 weeks, $P=0.008$ ) vs topotecan treatment (71.1 weeks) for platinum-sensitive patients with ovarian cancer <sup>14</sup>
		Metastatic breast cancer	No statistically significant overall survival change (84 weeks) vs conventional doxorubicin (88 weeks) for breast cancer patients receiving first-line therapy <sup>145</sup>
Liposomal daunorubicin	DaunoXome®	HIV-related Kaposi's sarcoma	No statistically significant overall survival change (52.7 weeks) vs doxorubicin, bleomycin and vincristine treatment (48.9 weeks) <sup>146</sup>
Albumin-bound paclitaxel	Abraxane®	Metastatic breast cancer	Statistically significant overall survival change (56.4 weeks, $P=0.024$ ) vs polyethylated castor oil-based paclitaxel treatment (46.7 weeks) for patients receiving second-line treatment <sup>7</sup>

\*The polymeric platform methoxy-PEG-poly(D,L-lactide) taxol with the trade name Genexol-PM (Samyang Co., Seoul, Korea) has been approved in Korea for the treatment of metastatic breast cancer.<sup>147,148</sup>

those in normal tissues (Figure 1a). Unlike normal vessels, tumor vessels lack an orderly branching hierarchy from large vessels into successively smaller vessels that feed a regularly spaced capillary bed. Instead, tumor vessels are heterogeneous in their spatial distribution, dilated and tortuous, leaving avascular spaces of various sizes.<sup>22,23</sup> In addition, in tumors, vessel-wall structure is abnormal with wide interendothelial junctions, an abnormally thick or thin basement membrane, large numbers of fenestrae and transendothelial channels formed by vesicles,<sup>24,25</sup> and

maximum pore diameters as large as several hundred nanometers (Figure 1b).<sup>26,27</sup> Owing to their irregular structure, vessel walls are leaky and hyperpermeable in some places while not in others. Finally, proliferating tumor cells and/or stromal cells exert solid stress and compress blood vessels, which might cause vessel collapse.<sup>28–30</sup>

As shown in Box 1, the elevated viscous and geometrical resistance offered by the vasculature can compromise tumor blood flow.<sup>22</sup> Therefore, the average velocity of red blood cells (RBCs) in tumor vessels can be an order of magnitude lower than in normal vessels and the overall perfusion rates (blood flow rate per unit volume) in tumors are reduced compared with many normal tissues (Figure 1c). Furthermore, unlike normal tissue, blood velocity in tumors is independent of vessel diameter and unevenly distributed, leaving poorly perfused or even unperfused regions.<sup>31–34</sup> The presence of unperfused regions leads to a hostile tumor microenvironment (for example, low partial oxygen pressure, low pH and necrotic tissue), which fuels drug resistance and tumor progression.

The normal lymphatic network drains excess fluid from tissue in order to maintain tissue interstitial fluid balance. In tumor tissue, the proliferating cancer cells compress lymphatic vessels, particularly at the center of the tumor, causing their collapse.<sup>28</sup> Therefore, functional lymphatic vessels exist only in the tumor periphery.<sup>35,36</sup> These peritumor lymphatics carry fluid, growth factors and cancer cells, and mediate tumor metastases via the lymphatic network (Figure 2a).<sup>37,38</sup> The inefficient drainage of fluid from the tumor center coupled with fluid leakage from tumor vessels contributes to interstitial hypertension.

Interstitial hypertension and impaired blood supply reduces the efficacy and delivery of therapeutic agents in solid tumors.<sup>16</sup> The subsequent hypoxia in tumor cells not only induces resistance to radiotherapy, but also causes resistance to several cytotoxic drugs. Independent of these effects, the genetic instability induced by hypoxia selects for cells with an increased potential for metastasis. The cytotoxic functions of immune cells that infiltrate a tumor are also compromised by both hypoxia and low pH. The fragile tumor vasculature may also facilitate the shedding of cancer cells into the circulation, which is a prerequisite for metastasis. Unfortunately, this abnormal tumor microenvironment does not impair tumor-cell survival.

In conclusion, the spatial and temporal heterogeneities in blood supply and vessel permeability along with poor lymphatic drainage help to create an abnormal microenvironment that impairs uniform delivery and efficacy of therapeutic agents in tumors.

**Abnormal vascular barrier**

There are at least five pathways for transport across the vascular endothelium: pathway one is diffusion through endothelial cells, two is lateral membrane diffusion, three is transport through intercellular junctions, four is transport through intracellular fenestrations (~40–60 nm), and, finally, five is vesicular transport (~100 nm).<sup>24</sup> Water and lipophilic solutes use pathways one, three and four for transport, and lipophilic solutes also cross the vascular endothelium by pathway two. Hydrophilic solutes and

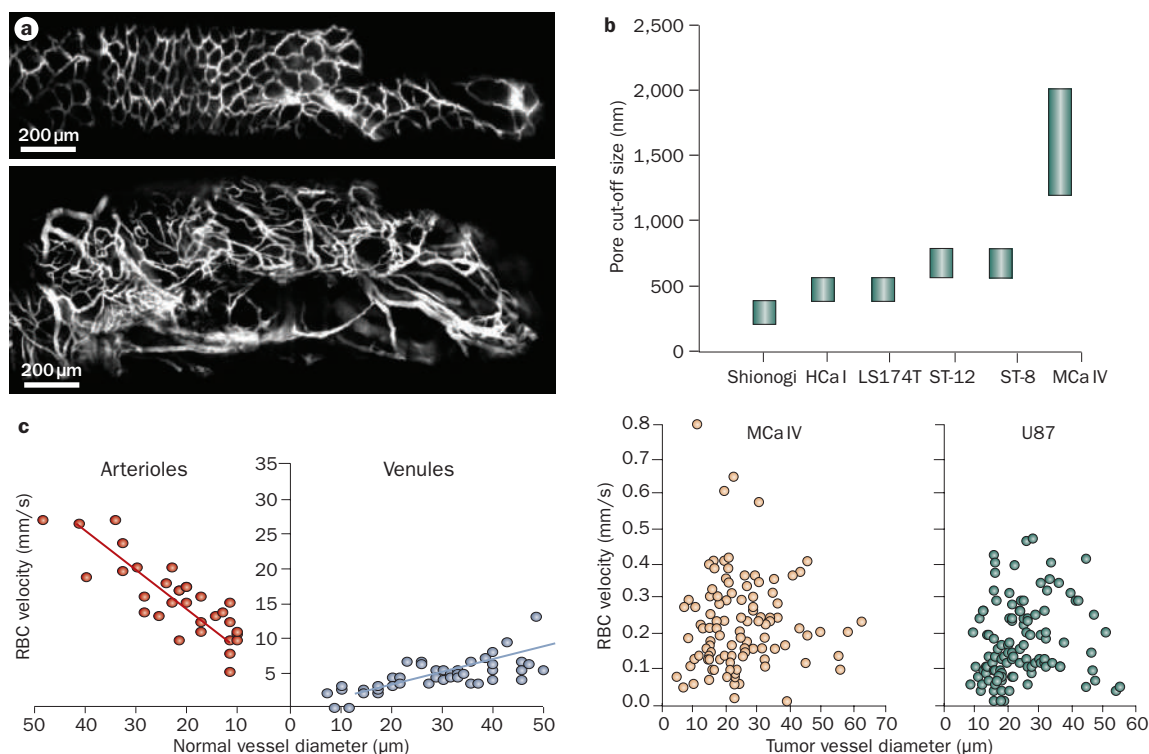


**Figure 1** | Vascular structure and function in tumors. **a** | Longitudinal fluorescence imaging of normal (top) and tumor (bottom) colon tissue in a floxed *Apc* mouse. Permission obtained from Nature Publishing Group © Kim, P. *et al. Nat. Methods* **7**, 303–305 (2010). **b** | Tumor vessels are leaky and have large pore sizes, which for some tumor types can be as large as a few micrometers in size. Permission obtained from the National Academy of Sciences, USA © Hobbs, S. K. *et al. Proc. Natl Acad. Sci. USA* **95**, 4607–4612 (1998). **c** | Blood velocity in normal pial vessels (left) and tumors (right) as a function of vessel diameter. Unlike normal tissue, in tumors blood velocity does not depend on vessel diameter. Permission obtained from the American Association of Cancer Research © Yuan, F. *et al. Cancer Res.* **54**, 4564–4568 (1994). Abbreviation: RBC, red blood cell.

macromolecules use pathways three and four, but macromolecules may also follow pathway five. Nanoparticles that are larger than albumin (~4 nm) are most likely to follow pathway three because interendothelial junctions in some tumors can be as large as a few micrometers.<sup>26,27</sup> The parameters that affect the extravasation of nanoparticles from the blood vessels are presented in Box 2.

Since tumor blood vessels have larger pores, the vascular permeability and hydraulic conductivity are significantly higher in tumor than in normal tissues;<sup>26,32,39–41</sup> this is the basis for the EPR effect.<sup>40,42</sup> Nanoparticles extravasate in tumor tissue from these large pores in tumor vessels. Vascular permeability decreases with the increase in the size of the transported particle.<sup>43,44</sup> Furthermore, cationic nanoparticles preferentially target tumor vessels and exhibit higher permeability compared with their anionic or neutral counterparts.<sup>45–49</sup> Vascular permeability depends not only on the properties of the particle, but also on the physiological characteristics of the vasculature. While using the EPR effect as a rationale for nanoparticles, it is often overlooked that not all tumor vessels are leaky, which causes a heterogeneous distribution of pore sizes and thus, heterogeneous extravasation and delivery.<sup>43,44,50</sup> In addition, the permeability in tumor models depends on the transplantation site and varies with time and in response to treatment.<sup>50–52</sup>

### Box 1 | Determinants of blood flow

Tumor blood flow,  $Q$ , is equal to the pressure difference between arterial and venous ends,  $\Delta P$ , divided by the flow resistance (FR). This is defined in the following equation:<sup>22</sup>

$$Q = \Delta P / FR$$

$FR = \eta Z$ , where  $\eta$  is the apparent viscosity (viscous resistance), and  $Z$  is the geometrical resistance.

Abnormalities in tumor vasculature increase both the geometric and viscous resistance to blood flow.<sup>22,149–151</sup> Geometric resistance is elevated because of the peculiar branching patterns of tumor vessels,<sup>152–154</sup> and their deformation due to compression by cancer cells.<sup>28,30</sup> Viscous resistance is elevated because tumors lose 5–10% of plasma as the blood flows from the arterial to venous side. This results in the increase of red blood cell concentration (hemoconcentration) that in turn increases the apparent viscosity.<sup>151,154,155</sup>

Another important barrier to transvascular transport is the elevated IFP that reduces pressure gradients across the vessel wall. In normal tissues, IFP is approximately 0 mmHg whereas tumors exhibit interstitial hypertension,<sup>15,38</sup> which is caused by the high permeability of tumor vessels in combination with the lack of functional lymphatic vessels in the tumor interstitial space.<sup>15,35</sup> As

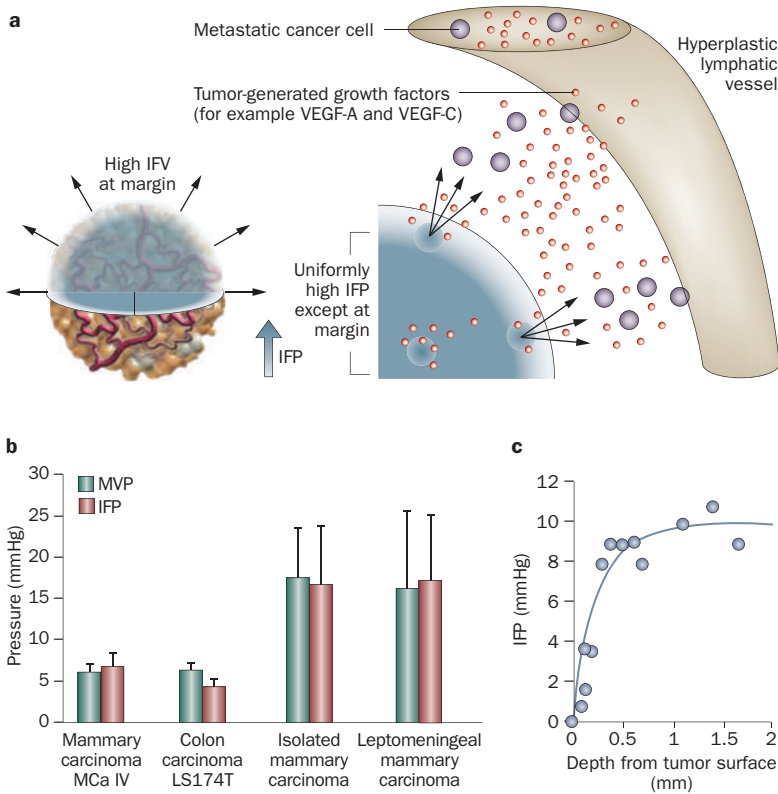


**Figure 2** | Elevated IFP in tumors. **a** | The IFP is uniformly elevated in tumors except at the margin. The steep drop of IFP at the margin causes fluid, growth factors and cells to leak out of the tumor into the peritumoral tissue, which in turn might facilitate angiogenesis and metastasis, and inhibit drug delivery. Permission obtained from American Association of Cancer Research © Jain, R. K. *et al. Cancer Res.* **67**, 2729–2735 (2007). **b** | The IFP and MVP for different tumor types. Permission obtained from the American Association of Cancer Research © Boucher, Y. & Jain, R. K. *Cancer Res.* **52**, 5110–5114 (1992) and © Boucher, Y. *et al. Cancer Res.* **56**, 4264–4266 (1996). **c** | IFP profile as a function of the distance from the tumor surface. Permission obtained from the American Association of Cancer Research © Boucher, Y. *et al. Cancer Res.* **50**, 4478–4484 (1990). Abbreviations: IFP, interstitial fluid pressure; IFV, interstitial fluid velocity; MVP, microvascular pressure.

a result, the IFP is uniformly elevated inside the tumor and becomes almost equal to the microvascular pressure (Figure 2b).<sup>17,53–57</sup> However, close to the tumor margin the IFP drops rapidly to normal values causing a steep pressure gradient (Figure 2c).<sup>53,58,59</sup> A direct consequence of the elevated IFP levels is that the main mechanism of mass transport across the vessel wall is diffusion, a process that is much slower than convection, particularly for large particles. It is also possible the IFP inside the tumor could transiently exceed the microvascular fluid pressure and, thus, cause intravasation of materials back to the blood supply.<sup>55</sup> Moreover, transmural coupling between microvascular pressure and IFP can abolish the pressure gradient along the length of a tumor vessel causing blood stasis in the absence of physical occlusions.<sup>60,61</sup> Finally, because of the steep drop in IFP, interstitial fluid escapes from the tumor periphery into the surrounding healthy tissue, carrying not only therapeutic nanoparticles but also growth factors (for example, VEGF-A, VEGF-C, platelet-derived growth factor [PDGF]-A and PDGF-C) and cells (for example, metastatic cancer cells) that fuel tumor progression.<sup>38,62</sup>

**Box 2** | Determinants of transvascular transport

Extravasation of materials from the blood vessels can occur by diffusion and convection and is described by the following equation:<sup>24</sup>

$$J = PS(C_p - C_i) + L_p S(1 - \sigma)[(p_v - p_i) - \sigma(\pi_v - \pi_i)]C_p$$

$J$  is the flux (mass per unit volume) of materials crossing the vessel wall,  $P$  is the vascular permeability,  $S$  is the vessels' surface area,  $C_p - C_i$  is the concentration difference of the material between the plasma and the interstitial space,  $L_p$  is the hydraulic conductivity of the vessel wall,  $p_v - p_i$  is the difference between microvascular and interstitial fluid pressure,  $\sigma$  is the osmotic reflection coefficient, and  $\pi_v - \pi_i$  is the osmotic pressure difference across the wall. The vascular permeability depends on the properties of the particle (size, charge and configuration) and the vessel wall (pore size, charge and arrangement). It decreases as the particle size increases and becomes zero when the particle size is larger than the pore cut-off size. The hydraulic conductivity is a property of the morphology of the wall and depends on the fraction of the wall surface occupied by pores. More comprehensive models for transvascular models exist but they are beyond the scope of this Review.

It is worth noting that the EPR effect (that is, increased vessel leakiness and impaired lymphatic function) is observed even during the early stages of carcinogenesis (for example, dysplasia and hyperplasia).<sup>63</sup> Thus, nanoparticles could be used to detect very small lesions for surgical removal.<sup>64,65</sup> However, the impairment of blood and lymphatic vessels could also pose a challenge for uniform delivery of nanoparticles throughout these lesions. Thus, the large size of nanoparticles along with the uniformly elevated IFP in tumors hinder transport across the vessel walls and compromise the benefits of the EPR effect.

**Abnormal interstitial barrier**

The parameters that govern the interstitial transport of nanoparticles in tumors are described in Box 3. The uniformly elevated IFP eliminates pressure gradients not only across the tumor vessel walls, but also inside the tumor. Therefore, the main mechanism of transport within tumors is diffusion. The tumor interstitial matrix consists of a highly interconnected network of collagen fibers that interact with other molecules, such as proteoglycans and glycosaminoglycans.<sup>66,67</sup> The movement of a diffusing nanoparticle depends on its size, charge and configuration as well as the physicochemical properties of the interstitial matrix.<sup>18</sup> Small therapeutic agents, such as chemotherapeutics, whose size is usually up to a few nanometers, diffuse fairly rapidly in the tumor interstitial matrix. However, the diffusion coefficient of nanoparticles, such as liposomes and viruses, whose size can be up to hundreds of nanometers in diameter, is considerably hindered by interactions with the interstitial matrix. Indeed, the extravascular space available for large therapeutic agents decreases with the size of the agents.<sup>68</sup> In addition, in many tumors, particles larger than 60 nm in diameter are not able to effectively diffuse through the collagen matrix.<sup>69–72</sup> These particles extravasate from blood vessels,

but because they cannot penetrate the tumor interstitial space, are concentrated around the vessels heterogeneously and cause only local effects (Figure 3a,b).<sup>43,73</sup> Charged particles develop electrostatic attraction or repulsion with charged components of the interstitial space that further hinders their diffusion, while macromolecules with linear, semi-flexible configuration diffuse more efficiently than do rigid spherical particles of comparable size.<sup>70,74</sup>

The collagen content is the major determinant of interstitial transport (Figure 3c).<sup>75–77</sup> Tumors rich in collagen hinder diffusion to a greater extent than tumors with a low collagen content. Also, the site of tumor growth plays a crucial role in the transport properties of the tumor.<sup>69</sup> As shown in Figure 3d, the same tumor type implanted in two different locations in mice (dorsal skin versus cranium) exhibits different diffusion coefficients, presumably because of different collagen levels.<sup>69</sup> Furthermore, collagen fibers carry a slightly positive charge at neutral pH, and thus may interact with negatively charged nanoparticles to form aggregates.<sup>78</sup>

Another determinant of interstitial transport is the sulfated glycosaminoglycan content. These thin and elongated fibers not only significantly increase the viscosity of the interstitial fluid, but they also carry a highly negative charge that—even in small quantities—can inhibit the transport of materials by forming aggregates.<sup>75,79–82</sup> For example, electrostatic binding between the diffusing nanoparticle and heparan sulfate can decrease the diffusion coefficient of the particle by three orders of magnitude.<sup>80,81</sup> However, this binding is reversible and enzymatic digestion of the heparan sulfate chains can rescue the mobility of the particle.

Finally, the heterogeneous distribution of the components of the interstitial matrix in the tumor separates the matrix in two phases—the viscous and the aqueous. The viscous phase is considered to be in regions of high collagen-fiber concentration and significantly hinders the particle mobility. The aqueous phase is found in low fiber-concentration regions where the diffusivity of the particle is similar to that in water. The two-phase nature of transport in the tumor matrix results in a two-component diffusion.<sup>72,83</sup> The fast component is associated with the aqueous phase, while the slow component is associated with the viscous phase. Consequently, the distributions of these phases greatly affect particle distribution in the tumor.

In conclusion, the dense and heterogeneous structure of the extracellular matrix in desmoplastic tumors blocks large nanotherapeutics and results in the heterogeneous distribution of these agents.

### Strategies to improve delivery

From the above evidence, we conclude that inefficient transport of diagnostic and therapeutic nanoparticles in tumors is a result of the abnormal structure and function of tumor vessels and the dense matrix associated with the desmoplastic response. Therefore, therapeutic strategies to enhance drug delivery have focused on normalizing the tumor vasculature to increase the efficiency of the vascular network, and normalizing the tumor interstitial

### Box 3 | Determinants of interstitial transport

Transport of nanoparticles through the interstitial matrix is governed by diffusion and convection:<sup>18</sup>

$$(\partial C_i / \partial t) + v \nabla C_i = D \nabla^2 C_i + R$$

$C_i$  is the nanoparticle concentration,  $v$  the interstitial fluid velocity,  $D$  the diffusion coefficient of the nanoparticles and  $R$  a term that accounts for binding or degradation of the nanoparticles. The fluid velocity depends on changes in the interstitial fluid pressure and because the latter is uniform in the center of the tumor, it is negligible except at the tumor margin. The diffusion coefficient depends on the properties of the nanoparticles (size, charge and configuration) and the structure of the interstitial matrix.

matrix so that nanoparticles penetrate faster and deeper inside the tumor.

### Normalization of tumor vasculature

New vessel formation in tumors is initiated by an imbalance of proangiogenic and antiangiogenic factors.<sup>16,84,85</sup> In normal tissues, the balance between these factors maintains the normal architecture of the vascular network in order to ensure optimal function. In tumors, however, proangiogenic molecules, (for example, VEGF, basic fibroblast growth factor and PDGF) are usually overexpressed, which tips the balance towards the proangiogenic side and causes the formation of chaotic blood vessels (Figure 4a). Therefore, judicious application of antiangiogenic agents can restore the balance and revert the vasculature to a more 'normal' phenotype.<sup>16,86</sup>

Of all the established proangiogenic molecules, VEGF seems to be the most critical and has been the focus of many studies. Blockade of VEGF causes pruning of immature vessels, decrease in vessel density and diameter, and remodeling of the vasculature to more closely resemble the structure of normal vessels.<sup>87,88</sup> More importantly, from the transport point of view, tumor vessels appear less tortuous and better perfused after treatment, and the IFP is significantly reduced, which restores pressure gradients across the vessel wall and leads to a deeper penetration of molecules into tumors and to improved oxygenation (Figure 4b–d).<sup>87,89,90</sup>

Agents with indirect antiangiogenic effects can also lead to vascular normalization. For example, trastuzumab significantly reduced the diameter, volume and permeability of tumor blood vessels, producing more normal networks by mimicking an antiangiogenic cocktail.<sup>91</sup> In another example, haploinsufficiency of the oxygen-sensing prolyl hydroxylase domain protein PHD2 normalized the endothelial lining resulting in reduced vessel leakiness and increased tumor perfusion and oxygenation.<sup>92,93</sup>

Tumor vascular normalization has been documented in rectal cancer patients receiving bevacizumab<sup>57</sup> and recurrent glioblastoma patients receiving cediranib.<sup>94</sup> IFP decreased by 70% 12 days after a single infusion of bevacizumab and vascular density decreased by 50%, causing a normalization of the tumor microenvironment and more efficient delivery of fluorodeoxyglucose (FDG). Patients with recurrent glioblastoma showed a rapid

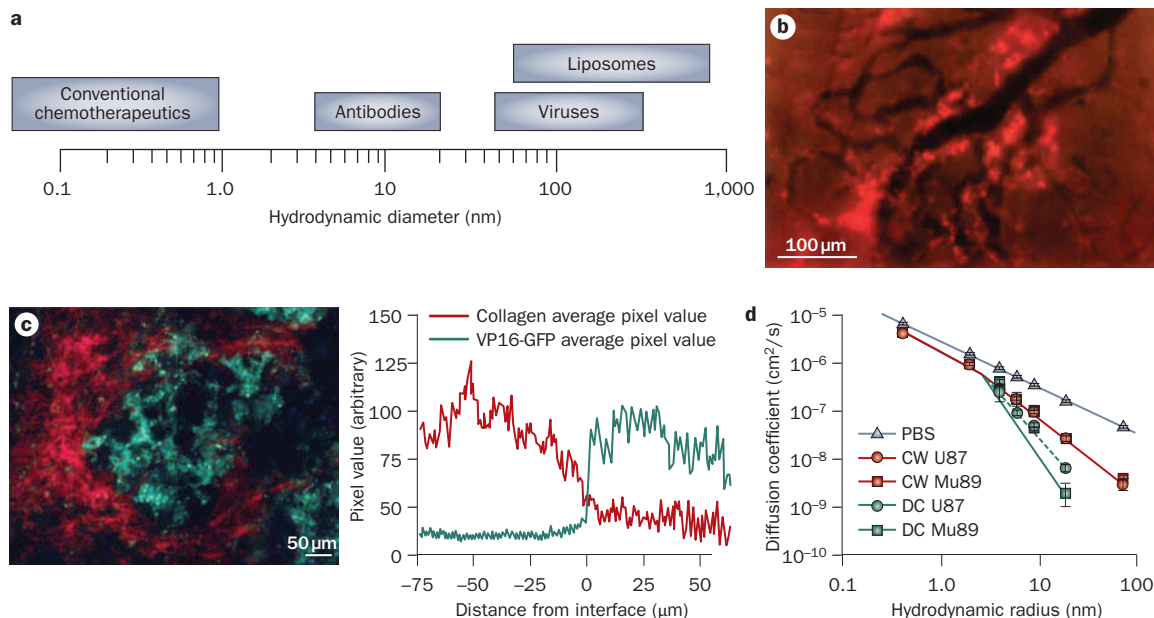


**Figure 3** | Barriers to interstitial transport of nanoparticles. **a** | The size of therapeutic agents can differ up to four orders of magnitude. **b** | The distribution of liposomes with a size of 90 nm in a tumor. The nanoparticles (bright red color) extravasate from some tumor blood vessels (black color) but because of their large size they cannot penetrate the tumor interstitial matrix and are concentrated in the perivascular region. Please note there is no extravasation from some vessels. Permission obtained from the American Association of Cancer Research © Yuan, F. *et al. Cancer Res.* **54**, 3352–3356 (1994). **c** | Diffusion of nanoparticles in the tumor interstitium depends on collagen content. At high collagen regions (red color) the concentration of herpes simplex virus (green color; with a size of 150 nm) is low, while at low collagen regions the concentration of the virus increases. Permission obtained from the American Association of Cancer Research © McKee, T. D. *et al. Cancer Res.* **66**, 2509–2513 (2006). **d** | Diffusion also depends on the implantation site. The plot depicts the diffusion coefficient of macromolecules in Mu89 melanomas and U87 glioblastomas implanted in the cranium and the dorsal skin. The diffusion coefficients in PBS solution are shown for comparison. Permission obtained from the National Academy of Sciences, USA © Pluen, A. *et al. Proc. Natl Acad. Sci. USA* **98**, 4628–4633 (2001). Abbreviations: CW, cranial window; DC, dorsal chamber; PBS, phosphate buffered saline.

normalization of the tumor microenvironment characterized by significant reduction in vascular permeability and vessel size.<sup>94</sup>

Vessel normalization might, however, compromise the transvascular transport of very large nanoparticles due to the decrease in the pore size of the vessel walls. The decrease of the pore size decreases the vascular permeability,  $P$ , and hydraulic conductivity,  $L_p$ , while it increases the reflection coefficient,  $\sigma$  (Box 2). The changes in these parameters decrease the particle flux across the vessel wall (Box 2) and might overwhelm the benefit gained by increasing perfusion and restoring the transmural pressure difference (Chauhan, V. P. *et al.* unpublished data). As an additional consideration, vessel normalization is transient, and thus, anticancer agents should be given during the window of normalization.<sup>16,88</sup> In addition to normalizing the structure and function of abnormal vessels, compressed vessels in tumors can be opened up and perfused by killing perivascular cancer cells<sup>28,30</sup> and stromal cells.<sup>95</sup> Unfortunately, these vessels become compressed again if the cancer or stromal cells regrow.

**Normalization of tumor matrix**

Penetration of molecules and nanoparticles in tumors depends on the volume fraction of the components of the

extracellular matrix, particularly the collagen and glycosaminoglycan content. To improve drug penetration we have attempted to degrade these components and thus increase the accessible volume to the diffusing particle.<sup>75</sup> Degradation of the collagen matrix with bacterial collagenase treatment in high collagen-content tumors (for example, HSTS26T sarcoma and Mu89 melanoma xenografts) caused a two-fold increase in the diffusion of antibodies, such as IgG (hydrodynamic radius 4.5 nm),<sup>72,75,96</sup> while the interstitial distribution of herpes simplex virus (HSV; hydrodynamic radius 75 nm) was increased by a factor of three (Figure 5a).<sup>73,97</sup> The distribution of HSV was also significantly increased by the ectopic expression of matrix metalloproteinase (MMP)-1 and MMP-8, which decreased the levels of tumor glycosaminoglycans and improved convection.<sup>79</sup> Bacterial collagenase, MMP-1 and MMP-8 considerably improved the antitumor efficacy of oncolytic HSV. The hormone relaxin, which modifies the structure of collagen fibers, can also increase transport by diffusion (Figure 5b).<sup>98,99</sup> Relaxin treatment caused a twofold increase in the diffusion of IgG and a threefold increase in the diffusion of dextran-2M (hydrodynamic radius 20 nm) in HSTS26T xenografts.<sup>98,99</sup> A recently discovered tumor penetrating peptide, iRGD, also has the potential to improve the delivery of nanotherapeutics in solid tumors by improving interstitial transport.<sup>100</sup>

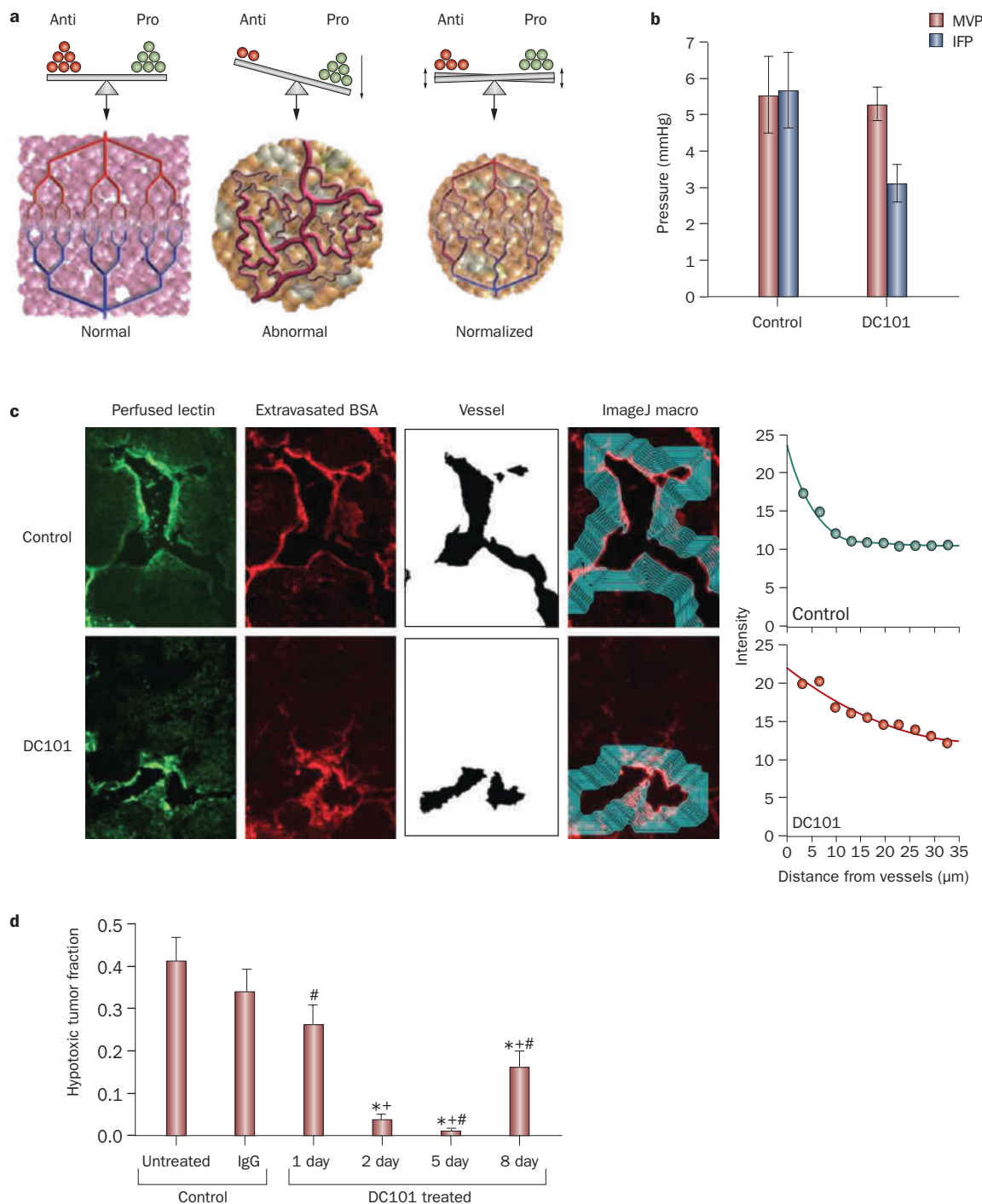


**Figure 4** | Effect of vascular normalization. **a** | Tumor angiogenesis results from an imbalance between antiangiogenic and proangiogenic factors. Normalization aims to restore this balance and bring the tumor vasculature to a more normal phenotype. Permission obtained from the American Association for the Advancement of Science © Jain, R. K. *Science* **307**, 58–62 (2005). **b** | Use of an anti-VEGF antibody, DC101, reduced IFP and had no effect on MVP. Permission obtained from the American Association of Cancer Research © Tong, R. T. *et al. Cancer Res.* **64**, 3731–3736 (2004). **c** | Frozen sections of murine mammary adenocarcinoma (MCAIV) tumors with perfused biotinylated lectin to identify functional vessels, and extravasated tetramethyl rhodamine isothiocyanate–BSA to study interstitial penetration. Vessels were identified using the ImageJ software and the average intensity of BSA was quantified as a function of distance from the blood vessel wall. Tumors treated with the antiangiogenic agent DC101 exhibited increased penetration of BSA in the tumor interstitial space. Permission obtained from the American Association of Cancer Research © Tong, R. T. *et al. Cancer Res.* **64**, 3731–3736 (2004). **d** | Normalization by DC101 decreased hypoxia in brain tumors in mice. Hypoxia reached a minimum at day 5, and a partial relapse occurred at day 8. \* $P < 0.05$ , compared with untreated control; \* $P < 0.05$ , compared with rat IgG-treated control (day 2); # $P < 0.05$ , compared with day 2 after initiation of DC101 therapy. Permission obtained from Elsevier Ltd. © Winkler, F. *et al. Cancer Cell* **6**, 553–563 (2004). Abbreviations: BSA, bovine serum albumin; IFP, interstitial fluid pressure; MVP, microvascular pressure.

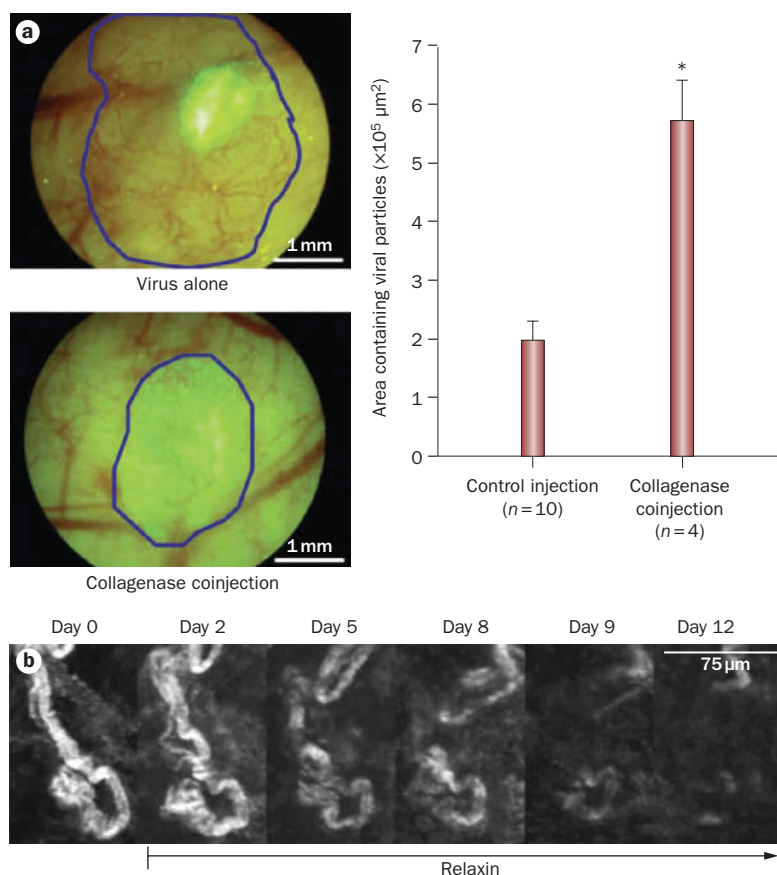


**Figure 5** | Effect of normalizing collagen matrix. **a** | Effect of interstitial matrix normalization on oncolytic viral therapy. Mu89 melanomas implanted in the dorsal skin-fold chamber were treated with the oncolytic vector MGH2 in combination with collagenase. Infection of tumor cells was detected by expression of the reporter gene *GFP* (encoded within the virus). Coinjection of MGH2 with collagenase increased cell infection and resulted in tumor regression (blue line). \* $P < 0.05$ . Permission obtained from the American Association of Cancer Research © McKee, T. D. *et al. Cancer Res.* **66**, 2509–2513 (2006). **b** | Effect of relaxin on collagen matrix in tumors. Second harmonic generation images of the collagen structure in a Mu89 melanoma during relaxin treatment. Maximum intensity projections of the same region of collagen fibers at different time points are shown. Relaxin treatment decreased collagen levels (white). Permission obtained from Nature Publishing Group © Brown, E. *et al. Nat. Med.* **9**, 796–800 (2003). Abbreviation: GFP, green fluorescent protein.

**Design considerations**

For optimal efficacy, a therapeutic agent must reach tumors in amounts sufficient to kill cancer cells but at the same time should not have adverse effects in normal tissues. Obviously, the smaller the particles the better the transport; however, small molecules, such as chemotherapeutics, generally extravasate in most normal tissues potentially causing adverse effects. The combination of the two constraints suggests that increasing the size of the nanoparticle will provide selectivity, but at the cost of limiting extravasation from some pores of tumor vessels and decreasing diffusion through the tumor matrix. Therefore, the size of the particle needs to be optimized for each tumor and its metastases. The challenge is that the tumor microenvironment is not spatially homogeneous and it changes with time and in response to treatment.

Not only the size but also the surface charge and the shape of therapeutic nanoparticles play a crucial role in extravasation and interstitial transport. On the one hand, it has been shown that cationic nanoparticles preferentially target tumor endothelial cells and exhibit a higher vascular permeability compared with their neutral or anionic counterparts.<sup>45–47</sup> On the other hand, neutral nanoparticles diffuse faster and distribute more homogeneously inside the tumor interstitial space than cationic and anionic particles, because the latter form aggregates with negatively charged (for example, hyaluronan) or positively charged (for example, collagen) matrix molecules.<sup>78,80</sup> As far as the particle shape is concerned, studies have shown that macromolecules with linear, semi-flexible configurations diffuse more efficiently in the interstitial matrix than do comparable sized, rigid spherical particles.<sup>70,74</sup>

The size of therapeutic particles also affects their circulation time in the blood stream. Provided the therapeutic agent is not toxic to normal tissues, it makes sense to prolong its half-life in the blood. The hydrodynamic diameter is inversely related to renal clearance. Particles with a hydrodynamic diameter smaller than 5–6 nm are rapidly cleared by the kidney (blood half-life <600 min), while increase in particle diameter can significantly increase the half-life of these agents in the blood and body.<sup>101,102</sup> As for the effect of nanoparticle shape on the circulation time, it has been shown that filamentous micelles have circulation times about 10 times longer than their spherical counterparts,<sup>103</sup> while filamentous nanotubes with very small diameters (<2 nm) have rapid renal clearance and circulation times of less than 3 h.<sup>104</sup> In addition to the kidneys, interaction between nanoparticles and the reticuloendothelial system in the liver and the spleen has an important role in nanoparticle clearance. Clearance from the reticuloendothelial system depends not only on particle size but also on surface modification and can vary significantly among the different types of nanoparticles.<sup>105,106</sup> As the surface charge becomes larger (either positive or negative), interactions with the reticuloendothelial system increase and lead to greater clearance of the particle. To achieve higher circulation times, modification with polyethylene glycols (PEGylation) is the most common approach. Nanoparticles are sterically stabilized by attaching PEGs to the surface and have surface charges that are slightly negative or positive. Steric stabilization prevents opsonization by serum proteins and phagocytosis by Kupffer cells or hepatocytes.<sup>107–109</sup>

Furthermore, if the nanoparticle requires intracellular delivery, cellular internalization would depend on size, configuration and charge. For spherical particles, it has been shown that internalization is faster for smaller particles and might follow a different mechanism than for larger particles.<sup>110,111</sup> In addition, researchers have found both experimentally and with the use of mathematical modeling that internalization is maximized for a range of particle sizes.<sup>112–114</sup> For example, for gold and silver nanoparticles in the size range of 2–100 nm, particles of sizes 40–50 nm were able to most effectively bind and induce receptor-mediated endocytic processes.<sup>115</sup> For non-spherical particles, it has been shown that the local

geometry of the particle at the contact point with the cell determines whether it will be internalized or not.<sup>116</sup> Specifically, internalization is more effective when rod-like particles align perpendicular to the cellular membrane as opposed to parallel alignment. Also, internalization is faster and more efficient for elongated particles (high aspect ratio), carrying a positive charge.<sup>117</sup> It should be noted, however, that many of the particles used in these studies were in the micrometer size range, much larger than the formulations used in nanomedicine. Thus, their relevance to the delivery of nanomedicine *in vivo* remains to be shown.

The efficacy of nanomedicine might be improved by constructing nanoparticles that respond to properties of the tumor microenvironment (for example, low pH and partial oxygen pressure, and activated MMPs; Figure 6) or to external forces (for example, electric pulses, magnetic field, ultrasound, heat and light).<sup>118</sup> Solid tumors have a lower interstitial pH than normal tissues,<sup>119</sup> and thus many pH-sensitive nanocarriers have been developed to deliver their drugs to tumors.<sup>120–123</sup> In addition, nanoparticle formulations have been developed that are activated by the enzymatic activity of proteinases in tumors.<sup>124–126</sup> The targeting of nanoparticles to tumors can also be achieved by the application of external sources, such as electric or magnetic fields,<sup>127–129</sup> ultrasound,<sup>130</sup> heat,<sup>131</sup> and light.<sup>132</sup> Furthermore, mesoporous silica particles have been developed that function as vehicles for the controlled release of therapeutic anticancer agents.<sup>133–135</sup>

Nanoparticles with targeting ligands (for example, monoclonal antibodies, their Fab fragments and other moieties) on their surface have been developed to specifically recognize and bind to the tumor vasculature or cancer cells.<sup>136</sup> The targeting of the tumor vasculature by nanoparticles armed with targeting peptides suppresses tumor growth and metastasis in mice.<sup>137–139</sup> Ligands that target cancer cells can increase the intracellular concentration and cytotoxicity of nanoparticles, however, the intratumoral penetration is not improved significantly compared with non-targeted drug delivery particles.<sup>140</sup> Tumor penetration is a passive process that requires a long circulating half-life to allow extravasation of the particle across the hyperpermeable tumor vessels and effective diffusion through the tumor interstitial space. The addition of targeting ligands increases the size and biological reactivity of the particles, which exacerbates the problem of transport across these barriers. There are, however, cases where targeted nanoparticles have been proven to increase penetration. Coating of abraxane with the Lyp-1 or iRGD peptide increased drug penetration and, thus, the efficacy of the treatment.<sup>139,141</sup> In addition, another nanoparticle formulation has been recently shown to effectively deliver siRNA to humans.<sup>10</sup> The challenge now is to deliver the nanoparticle uniformly throughout a tumor and its

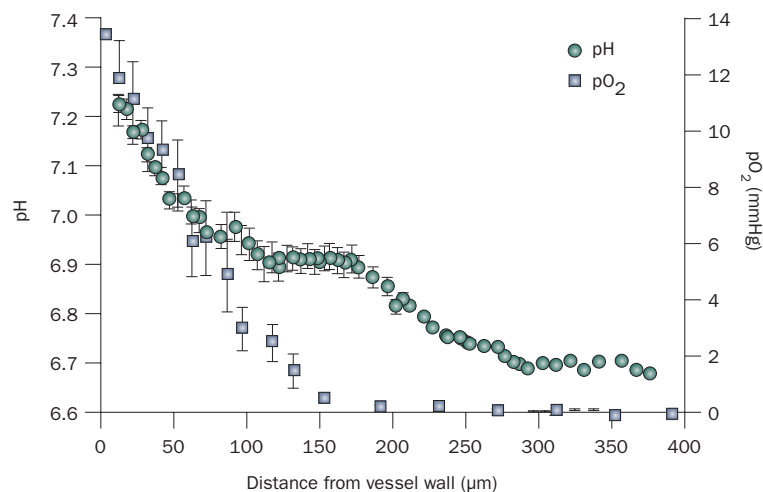


**Figure 6** | Mean interstitial pH and  $pO_2$  as a function of the distance to the nearest blood vessel. Please note the low pH and low  $pO_2$  only becomes significantly low beyond  $100\ \mu\text{m}$  from a blood vessel wall. Thus, pH sensitive particles need to penetrate beyond  $100\ \mu\text{m}$  to take advantage of the low pH. Permission obtained from Nature Publishing Group © Helmlinger, G. *et al. Nat. Med.* **3**, 177–182 (1997). Abbreviation:  $pO_2$ , partial oxygen pressure.

metastases given the limitations of spatial and temporal changes in the expression of the target.

## Conclusions

With increasing numbers of nanoparticles in preclinical and clinical studies for cancer detection and therapy, it is critical to consider the physiological barriers that hinder their delivery and develop strategies that can overcome these barriers. This coordinated approach will help to determine design criteria that optimize delivery. Given the highly heterogeneous and continuously evolving nature of the tumor microenvironment, the optimal design of nanoparticles is likely to be disease specific. This is a formidable task, especially considering the difference from one tumor to the next, from primary tumor to its metastasis, from one day to the next in the same tumor and the changes induced by treatment. In this Review, we proposed some basic guidelines for the construction of nanotherapeutics based on approaches that reduce this heterogeneity.

### Review criteria

Information for this Review was compiled by searching the PubMed and Web of Science databases for articles published before 6 June 2010, including early-release publications. Search terms included “barriers drug delivery tumors”, “nanomedicine delivery barriers”, “vessel normalization tumor”, and “nanoparticle clearance cancer”. Full articles were checked for additional material when appropriate, and articles that cite key publications were also checked.

1. Torchilin, V. P Targeted pharmaceutical nanocarriers for cancer therapy and imaging. *AAPS J.* **9**, E128–E147 (2007).
2. Schroeder, A., Levins, C. G., Cortez, C., Langer, R. & Anderson, D. G. Lipid-based nanotherapeutics for siRNA delivery. *J. Intern. Med.* **267**, 9–21 (2010).
3. Wagner, V., Dullaart, A., Bock, A. K. & Zweck, A. The emerging nanomedicine landscape. *Nat. Biotechnol.* **24**, 1211–1217 (2006).
4. Duncan, R. Polymer conjugates as anticancer nanomedicines. *Nat. Rev. Cancer* **6**, 688–701 (2006).
5. Stroh, M. *et al.* Quantum dots spectrally distinguish multiple species within the tumor milieu *in vivo*. *Nat. Med.* **11**, 678–682 (2005).
6. Allen, P. M. *et al.* InAs(ZnCdS) quantum dots optimized for biological imaging in the near-infrared. *J. Am. Chem. Soc.* **132**, 470–471 (2010).

7. Gradishar, W. J. *et al.* Phase III trial of nanoparticle albumin-bound paclitaxel compared with polyethylated castor oil-based paclitaxel in women with breast cancer. *J. Clin. Oncol.* **23**, 7794–7803 (2005).
8. Gelderblom, H., Verweij, J., Nooter, K. & Sparreboom, A. Cremophor EL: the drawbacks and advantages of vehicle selection for drug formulation. *Eur. J. Cancer* **37**, 1590–1598 (2001).
9. Weiss, R. B. *et al.* Hypersensitivity reactions from taxol. *J. Clin. Oncol.* **8**, 1263–1268 (1990).
10. Davis, M. E. *et al.* Evidence of RNAi in humans from systemically administered siRNA via targeted nanoparticles. *Nature* **464**, 1067–1070 (2010).
11. Hu, C. M. & Zhang, L. Therapeutic nanoparticles to combat cancer drug resistance. *Curr. Drug Metab.* **10**, 836–841 (2009).
12. Zhang, L. *et al.* Nanoparticles in medicine: therapeutic applications and developments. *Clin. Pharmacol. Ther.* **83**, 761–769 (2008).
13. Davis, M. E., Chen, Z. G. & Shin, D. M. Nanoparticle therapeutics: an emerging treatment modality for cancer. *Nat. Rev. Drug Discov.* **7**, 771–782 (2008).
14. Gordon, A. N. *et al.* Recurrent epithelial ovarian carcinoma: a randomized phase III study of pegylated liposomal doxorubicin versus topotecan. *J. Clin. Oncol.* **19**, 3312–3322 (2001).
15. Jain, R. K. Barriers to drug delivery in solid tumors. *Sci. Am.* **271**, 58–65 (1994).
16. Jain, R. K. Normalization of tumor vasculature: an emerging concept in antiangiogenic therapy. *Science* **307**, 58–62 (2005).
17. Boucher, Y., Baxter, L. T. & Jain, R. K. Interstitial pressure gradients in tissue-isolated and subcutaneous tumors: implications for therapy. *Cancer Res.* **50**, 4478–4484 (1990).
18. Jain, R. K. Transport of molecules in the tumor interstitium: a review. *Cancer Res.* **47**, 3039–3051 (1987).
19. Gazit, Y., Berk, D. A., Leunig, M., Baxter, L. T. & Jain, R. K. Scale-invariant behavior and vascular network formation in normal and tumor tissue. *Phys. Rev. Lett.* **75**, 2428–2431 (1995).
20. Baxter, L. T. & Jain, R. K. Transport of fluid and macromolecules in tumors. II. Role of heterogeneous perfusion and lymphatics. *Microvasc. Res.* **40**, 246–263 (1990).
21. Baish, J. W. *et al.* Role of tumor vascular architecture in nutrient and drug delivery: an invasion percolation-based network model. *Microvasc. Res.* **51**, 327–346 (1996).
22. Jain, R. K. Determinants of tumor blood flow: a review. *Cancer Res.* **48**, 2641–2658 (1988).
23. Vakoc, B. J. *et al.* Three-dimensional microscopy of the tumor microenvironment *in vivo* using optical frequency domain imaging. *Nat. Med.* **15**, 1219–1223 (2009).
24. Jain, R. K. Transport of molecules across tumor vasculature. *Cancer Metastasis Rev.* **6**, 559–593 (1987).
25. Roberts, W. G. & Palade, G. E. Neovasculature induced by vascular endothelial growth factor is fenestrated. *Cancer Res.* **57**, 765–772 (1997).
26. Hobbs, S. K. *et al.* Regulation of transport pathways in tumor vessels: role of tumor type and microenvironment. *Proc. Natl Acad. Sci. USA* **95**, 4607–4612 (1998).
27. Hashizume, H. *et al.* Openings between defective endothelial cells explain tumor vessel leakiness. *Am. J. Pathol.* **156**, 1363–1380 (2000).
28. Padera, T. P. *et al.* Pathology: cancer cells compress intratumour vessels. *Nature* **427**, 695 (2004).
29. Roose, T., Netti, P. A., Munn, L. L., Boucher, Y. & Jain, R. K. Solid stress generated by spheroid growth estimated using a linear poroelasticity model. *Microvasc. Res.* **66**, 204–212 (2003).
30. Griffon-Etienne, G., Boucher, Y., Brekken, C., Suit, H. D. & Jain, R. K. Taxane-induced apoptosis decompresses blood vessels and lowers interstitial fluid pressure in solid tumors: clinical implications. *Cancer Res.* **59**, 3776–3782 (1999).
31. Leunig, M. *et al.* Angiogenesis, microvascular architecture, microhemodynamics, and interstitial fluid pressure during early growth of human adenocarcinoma LS174T in SCID mice. *Cancer Res.* **52**, 6553–6560 (1992).
32. Yuan, F. *et al.* Vascular permeability and microcirculation of gliomas and mammary carcinomas transplanted in rat and mouse cranial windows. *Cancer Res.* **54**, 4564–4568 (1994).
33. Kamoun, W. S. *et al.* Simultaneous measurement of RBC velocity, flux, hematocrit and shear rate in vascular networks *in vivo*. *Nat. Methods* **7**, 655–660 (2010).
34. Endrich, B., Reinhold, H. S., Gross, J. F. & Intaglietta, M. Tissue perfusion inhomogeneity during early tumor growth in rats. *J. Natl Cancer Inst.* **62**, 387–395 (1979).
35. Padera, T. P. *et al.* Lymphatic metastasis in the absence of functional intratumor lymphatics. *Science* **296**, 1883–1886 (2002).
36. Leu, A. J., Berk, D. A., Lymboussaki, A., Alitalo, K. & Jain, R. K. Absence of functional lymphatics within a murine sarcoma: a molecular and functional evaluation. *Cancer Res.* **60**, 4324–4327 (2000).
37. Hoshida, T. *et al.* Imaging steps of lymphatic metastasis reveals that vascular endothelial growth factor-C increases metastasis by increasing delivery of cancer cells to lymph nodes: therapeutic implications. *Cancer Res.* **66**, 8065–8075 (2006).
38. Jain, R. K., Tong, R. T. & Munn, L. L. Effect of vascular normalization by antiangiogenic therapy on interstitial hypertension, peritumor edema, and lymphatic metastasis: insights from a mathematical model. *Cancer Res.* **67**, 2729–2735 (2007).
39. Dvorak, H. F., Brown, L. F., Detmar, M. & Dvorak, A. M. Vascular permeability factor/vascular endothelial growth factor, microvascular hyperpermeability, and angiogenesis. *Am. J. Pathol.* **146**, 1029–1039 (1995).
40. Gerlowski, L. E. & Jain, R. K. Microvascular permeability of normal and neoplastic tissues. *Microvasc. Res.* **31**, 288–305 (1986).
41. Sevic, E. M. & Jain, R. K. Measurement of capillary filtration coefficient in a solid tumor. *Cancer Res.* **51**, 1352–1355 (1991).
42. Maeda, H., Wu, J., Sawa, T., Matsumura, Y. & Hori, K. Tumor vascular permeability and the EPR effect in macromolecular therapeutics: a review. *J. Control. Release* **65**, 271–284 (2000).
43. Yuan, F. *et al.* Microvascular permeability and interstitial penetration of sterically stabilized (stealth) liposomes in a human tumor xenograft. *Cancer Res.* **54**, 3352–3356 (1994).
44. Yuan, F. *et al.* Vascular permeability in a human tumor xenograft: molecular size dependence and cutoff size. *Cancer Res.* **55**, 3752–3756 (1995).
45. Campbell, R. B. *et al.* Cationic charge determines the distribution of liposomes between the vascular and extravascular compartments of tumors. *Cancer Res.* **62**, 6831–6836 (2002).
46. Schmitt-Sody, M. *et al.* Neovascular targeting therapy: paclitaxel encapsulated in cationic liposomes improves antitumoral efficacy. *Clin. Cancer Res.* **9**, 2335–2341 (2003).
47. Dellian, M., Yuan, F., Trubetskov, V. S., Torchilin, V. P. & Jain, R. K. Vascular permeability in a human tumor xenograft: molecular charge dependence. *Br. J. Cancer* **82**, 1513–1518 (2000).
48. Thurston, G. *et al.* Cationic liposomes target angiogenic endothelial cells in tumors and chronic inflammation in mice. *J. Clin. Invest.* **101**, 1401–1413 (1998).
49. Krasnici, S. *et al.* Effect of the surface charge of liposomes on their uptake by angiogenic tumor vessels. *Int. J. Cancer* **105**, 561–567 (2003).
50. Yuan, F. *et al.* Time-dependent vascular regression and permeability changes in established human tumor xenografts induced by an anti-vascular endothelial growth factor/vascular permeability factor antibody. *Proc. Natl Acad. Sci. USA* **93**, 14765–14770 (1996).
51. Fukumura, D., Yuan, F., Monsky, W. L., Chen, Y. & Jain, R. K. Effect of host microenvironment on the microcirculation of human colon adenocarcinoma. *Am. J. Pathol.* **151**, 679–688 (1997).
52. Monsky, W. L. *et al.* Role of host microenvironment in angiogenesis and microvascular functions in human breast cancer xenografts: mammary fat pad versus cranial tumors. *Clin. Cancer Res.* **8**, 1008–1013 (2002).
53. Baxter, L. T. & Jain, R. K. Transport of fluid and macromolecules in tumors. I. Role of interstitial pressure and convection. *Microvasc. Res.* **37**, 77–104 (1989).
54. Boucher, Y., Kirkwood, J. M., Opacic, D., Desantis, M. & Jain, R. K. Interstitial hypertension in superficial metastatic melanomas in humans. *Cancer Res.* **51**, 6691–6694 (1991).
55. Boucher, Y. & Jain, R. K. Microvascular pressure is the principal driving force for interstitial hypertension in solid tumors: implications for vascular collapse. *Cancer Res.* **52**, 5110–5114 (1992).
56. Less, J. R. *et al.* Interstitial hypertension in human breast and colorectal tumors. *Cancer Res.* **52**, 6371–6374 (1992).
57. Willett, C. G. *et al.* Direct evidence that the VEGF-specific antibody bevacizumab has antivascular effects in human rectal cancer. *Nat. Med.* **10**, 145–147 (2004).
58. Jain, R. K. & Baxter, L. T. Mechanisms of heterogeneous distribution of monoclonal antibodies and other macromolecules in tumors: significance of elevated interstitial pressure. *Cancer Res.* **48**, 7022–7032 (1988).
59. Baxter, L. T. & Jain, R. K. Transport of fluid and macromolecules in tumors. IV. A microscopic model of the perivascular distribution. *Microvasc. Res.* **41**, 252–272 (1991).
60. Netti, P. A., Roberge, S., Boucher, Y., Baxter, L. T. & Jain, R. K. Effect of transvascular fluid exchange on pressure-flow relationship in tumors: a proposed mechanism for tumor blood flow heterogeneity. *Microvasc. Res.* **52**, 27–46 (1996).
61. Baish, J. W., Netti, P. A. & Jain, R. K. Transmural coupling of fluid flow in microcirculatory network and interstitium in tumors. *Microvasc. Res.* **53**, 128–141 (1997).
62. Lichtenbeld, H. C., Yuan, F., Michel, C. C. & Jain, R. K. Perfusion of single tumor microvessels: application to vascular permeability measurement. *Microcirculation* **3**, 349–357 (1996).
63. Hagendoorn, J. *et al.* Onset of abnormal blood and lymphatic vessel function and interstitial hypertension in early stages of carcinogenesis. *Cancer Res.* **66**, 3360–3364 (2006).

64. Nguyen, Q. T. *et al.* Surgery with molecular fluorescence imaging using activatable cell-penetrating peptides decreases residual cancer and improves survival. *Proc. Natl Acad. Sci. USA* **107**, 4317–4322 (2010).
65. Olson, E. S. *et al.* Activatable cell penetrating peptides linked to nanoparticles as dual probes for *in vivo* fluorescence and MR imaging of proteases. *Proc. Natl Acad. Sci. USA* **107**, 4311–4316 (2010).
66. Dvorak, H. F. Tumors: wounds that do not heal. Similarities between tumor stroma generation and wound healing. *N. Engl. J. Med.* **315**, 1650–1659 (1986).
67. Ronnov-Jessen, L., Petersen, O. W. & Bissell, M. J. Cellular changes involved in conversion of normal to malignant breast: importance of the stromal reaction. *Physiol. Rev.* **76**, 69–125 (1996).
68. Krol, A., Maresca, J., Dewhirst, M. W. & Yuan, F. Available volume fraction of macromolecules in the extravascular space of a fibrosarcoma: implications for drug delivery. *Cancer Res.* **59**, 4136–4141 (1999).
69. Pluen, A. *et al.* Role of tumor–host interactions in interstitial diffusion of macromolecules: cranial vs. subcutaneous tumors. *Proc. Natl Acad. Sci. USA* **98**, 4628–4633 (2001).
70. Pluen, A., Netti, P. A., Jain, R. K. & Berk, D. A. Diffusion of macromolecules in agarose gels: comparison of linear and globular configurations. *Biophys. J.* **77**, 542–552 (1999).
71. Ramanujan, S. *et al.* Diffusion and convection in collagen gels: implications for transport in the tumor interstitium. *Biophys. J.* **83**, 1650–1660 (2002).
72. Alexandrakis, G. *et al.* Two-photon fluorescence correlation microscopy reveals the two-phase nature of transport in tumors. *Nat. Med.* **10**, 203–207 (2004).
73. McKee, T. D. *et al.* Degradation of fibrillar collagen in a human melanoma xenograft improves the efficacy of an oncolytic herpes simplex virus vector. *Cancer Res.* **66**, 2509–2513 (2006).
74. Nugent, L. J. & Jain, R. K. Extravascular diffusion in normal and neoplastic tissues. *Cancer Res.* **44**, 238–244 (1984).
75. Netti, P. A., Berk, D. A., Swartz, M. A., Grodzinsky, A. J. & Jain, R. K. Role of extracellular matrix assembly in interstitial transport in solid tumors. *Cancer Res.* **60**, 2497–2503 (2000).
76. Choi, J. *et al.* Intraperitoneal immunotherapy for metastatic ovarian carcinoma: resistance of intratumoral collagen to antibody penetration. *Clin. Cancer Res.* **12**, 1906–1912 (2006).
77. Stylianopoulos, T., Diop-Frimpong, B., Munn, L. L. & Jain, R. K. Diffusion anisotropy in collagen gels and tumors: the effect of fiber network orientation. *Biophys. J.* (in press).
78. Stylianopoulos, T. *et al.* Diffusion of particles in the extracellular matrix: the effect of repulsive electrostatic interactions. *Biophys. J.* (in press).
79. Mok, W., Boucher, Y. & Jain, R. K. Matrix metalloproteinases-1 and -8 improve the distribution and efficacy of an oncolytic virus. *Cancer Res.* **67**, 10664–10668 (2007).
80. Lieleg, O., Baumgartel, R. M. & Bausch, A. R. Selective filtering of particles by the extracellular matrix: an electrostatic bandpass. *Biophys. J.* **97**, 1569–1577 (2009).
81. Thorne, R. G., Lakkaraju, A., Rodriguez-Boulan, E. & Nicholson, C. *In vivo* diffusion of lactoferrin in brain extracellular space is regulated by interactions with heparan sulfate. *Proc. Natl Acad. Sci. USA* **105**, 8416–8421 (2008).
82. Dowd, C. J., Cooney, C. L. & Nugent, M. A. Heparan sulfate mediates bFGF transport through basement membrane by diffusion with rapid reversible binding. *J. Biol. Chem.* **274**, 5236–5244 (1999).
83. Chauhan, V. P. *et al.* Multiscale measurements distinguish cellular and interstitial hindrances to diffusion *in vivo*. *Biophys. J.* **97**, 330–336 (2009).
84. Carmeliet, P. & Jain, R. K. Angiogenesis in cancer and other diseases. *Nature* **407**, 249–257 (2000).
85. Yancopoulos, G. D. *et al.* Vascular-specific growth factors and blood vessel formation. *Nature* **407**, 242–248 (2000).
86. Jain, R. K. Normalizing tumor vasculature with anti-angiogenic therapy: a new paradigm for combination therapy. *Nat. Med.* **7**, 987–989 (2001).
87. Tong, R. T. *et al.* Vascular normalization by vascular endothelial growth factor receptor 2 blockade induces a pressure gradient across the vasculature and improves drug penetration in tumors. *Cancer Res.* **64**, 3731–3736 (2004).
88. Winkler, F. *et al.* Kinetics of vascular normalization by VEGFR2 blockade governs brain tumor response to radiation: role of oxygenation, angiopoietin-1, and matrix metalloproteinases. *Cancer Cell* **6**, 553–563 (2004).
89. Wildiers, H. *et al.* Effect of anti-vascular endothelial growth factor treatment on the intratumoral uptake of CPT-11. *Br. J. Cancer* **88**, 1979–1986 (2003).
90. Lee, C. G. *et al.* Anti-vascular endothelial growth factor treatment augments tumor radiation response under normoxic or hypoxic conditions. *Cancer Res.* **60**, 5565–5570 (2000).
91. Izumi, Y., Xu, L., di Tomaso, E., Fukumura, D. & Jain, R. K. Tumour biology: herceptin acts as an anti-angiogenic cocktail. *Nature* **416**, 279–280 (2002).
92. Mazzone, M. *et al.* Heterozygous deficiency of PHD2 restores tumor oxygenation and inhibits metastasis via endothelial normalization. *Cell* **136**, 839–851 (2009).
93. Jain, R. K. A new target for tumor therapy. *N. Engl. J. Med.* **360**, 2669–2671 (2009).
94. Batchelor, T. T. *et al.* AZD2171, a pan-VEGF receptor tyrosine kinase inhibitor, normalizes tumor vasculature and alleviates edema in glioblastoma patients. *Cancer Cell* **11**, 83–95 (2007).
95. Olive, K. P. *et al.* Inhibition of Hedgehog signaling enhances delivery of chemotherapy in a mouse model of pancreatic cancer. *Science* **324**, 1457–1461 (2009).
96. Magzoub, M., Jin, S. & Verkmann, A. S. Enhanced macromolecule diffusion deep in tumors after enzymatic digestion of extracellular matrix collagen and its associated proteoglycan decorin. *FASEB J.* **22**, 276–284 (2008).
97. Mok, W., Stylianopoulos, T., Boucher, Y. & Jain, R. K. Mathematical modeling of herpes simplex virus distribution in solid tumors: implications for cancer gene therapy. *Clin. Cancer Res.* **15**, 2352–2360 (2009).
98. Brown, E. *et al.* Dynamic imaging of collagen and its modulation in tumors *in vivo* using second-harmonic generation. *Nat. Med.* **9**, 796–800 (2003).
99. Perentes, J. Y. *et al.* *In vivo* imaging of extracellular matrix remodeling by tumor-associated fibroblasts. *Nat. Methods* **6**, 143–145 (2009).
100. Sugahara, K. N. *et al.* Coadministration of a tumor-penetrating peptide enhances the efficacy of cancer drugs. *Science* **328**, 1031–1035 (2010).
101. Choi, H. S. *et al.* Renal clearance of quantum dots. *Nat. Biotechnol.* **25**, 1165–1170 (2007).
102. Choi, H. S. *et al.* Design considerations for tumour-targeted nanoparticles. *Nat. Nanotechnol.* **5**, 42–47 (2010).
103. Geng, Y. *et al.* Shape effects of filaments versus spherical particles in flow and drug delivery. *Nat. Nanotechnol.* **2**, 249–255 (2007).
104. Singh, R. *et al.* Tissue biodistribution and blood clearance rates of intravenously administered carbon nanotube radiotracers. *Proc. Natl Acad. Sci. USA* **103**, 3357–3362 (2006).
105. Longmire, M., Choyke, P. L. & Kobayashi, H. Clearance properties of nano-sized particles and molecules as imaging agents: considerations and caveats. *Nanomedicine (Lond.)* **3**, 703–717 (2008).
106. Franzen, S. & Lommel, S. A. Targeting cancer with ‘smart bombs’: equipping plant virus nanoparticles for a ‘seek and destroy’ mission. *Nanomedicine (Lond.)* **4**, 575–588 (2009).
107. Klibanov, A. L., Maruyama, K., Torchilin, V. P. & Huang, L. Amphipathic polyethylene glycols effectively prolong the circulation time of liposomes. *FEBS Lett.* **268**, 235–237 (1990).
108. Peracchia, M. T. *et al.* Stealth PEGylated polycyanoacrylate nanoparticles for intravenous administration and splenic targeting. *J. Control. Release* **60**, 121–128 (1999).
109. Storm, G., Belliot, S. O., Daemen, T. & Lasic, D. D. Surface modification of nanoparticles to oppose uptake by the mononuclear phagocyte system. *Adv. Drug Deliv. Rev.* **17**, 31–48 (1995).
110. Decuzzi, P., Pasqualini, R., Arap, W. & Ferrari, M. Intravascular delivery of particulate systems: does geometry really matter? *Pharm. Res.* **26**, 235–243 (2009).
111. Rejman, J., Oberle, V., Zuhorn, I. S. & Hoekstra, D. Size-dependent internalization of particles via the pathways of clathrin- and caveolae-mediated endocytosis. *Biochem. J.* **377**, 159–169 (2004).
112. Chithrani, B. D., Ghazani, A. A. & Chan, W. C. Determining the size and shape dependence of gold nanoparticle uptake into mammalian cells. *Nano. Lett.* **6**, 662–668 (2006).
113. Gao, H., Shi, W. & Freund, L. B. Mechanics of receptor-mediated endocytosis. *Proc. Natl Acad. Sci. USA* **102**, 9469–9474 (2005).
114. Foged, C., Brodin, B., Frokjaer, S. & Sundblad, A. Particle size and surface charge affect particle uptake by human dendritic cells in an *in vitro* model. *Int. J. Pharm.* **298**, 315–322 (2005).
115. Jiang, W., Kim, B. Y., Rutka, J. T. & Chan, W. C. Nanoparticle-mediated cellular response is size-dependent. *Nat. Nanotechnol.* **3**, 145–150 (2008).
116. Champion, J. A. & Mitragotri, S. Role of target geometry in phagocytosis. *Proc. Natl Acad. Sci. USA* **103**, 4930–4934 (2006).
117. Gratton, S. E. *et al.* The effect of particle design on cellular internalization pathways. *Proc. Natl Acad. Sci. USA* **105**, 11613–11618 (2008).
118. Wagner, E. Programmed drug delivery: nanosystems for tumor targeting. *Expert Opin. Biol. Ther.* **7**, 587–593 (2007).
119. Helmlinger, G., Yuan, F., Dellian, M. & Jain, R. K. Interstitial pH and pO<sub>2</sub> gradients in solid tumors *in vivo*: high-resolution measurements reveal a lack of correlation. *Nat. Med.* **3**, 177–182 (1997).
120. Kale, A. A. & Torchilin, V. P. Environment-responsive multifunctional liposomes. *Methods Mol. Biol.* **605**, 213–242 (2010).
121. Meyer, O., Papahadjopoulos, D. & Leroux, J. C. Copolymers of N-isopropylacrylamide can trigger pH sensitivity to stable liposomes. *FEBS Lett.* **421**, 61–64 (1998).

122. Leroux, J., Roux, E., Le Garrec, D., Hong, K. & Drummond, D. C. N-isopropylacrylamide copolymers for the preparation of pH-sensitive liposomes and polymeric micelles. *J. Control. Release* **72**, 71–84 (2001).
123. Meyer, M. & Wagner, E. pH-responsive shielding of non-viral gene vectors. *Expert Opin. Drug Deliv.* **3**, 563–571 (2006).
124. Harris, T. J., von Maltzahn, G., Derfus, A. M., Ruoslahti, E. & Bhatia, S. N. Proteolytic actuation of nanoparticle self-assembly. *Angew. Chem. Int. Ed. Engl.* **45**, 3161–3165 (2006).
125. Lee, S. *et al.* A near-infrared-fluorescence-quenched gold-nanoparticle imaging probe for *in vivo* drug screening and protease activity determination. *Angew. Chem. Int. Ed. Engl.* **47**, 2804–2807 (2008).
126. Mu, C. J., Lavan, D. A., Langer, R. S. & Zetter, B. R. Self-assembled gold nanoparticle molecular probes for detecting proteolytic activity *in vivo*. *ACS Nano* **4**, 1511–1520 (2010).
127. Goto, T. *et al.* Highly efficient electro-gene therapy of solid tumor by using an expression plasmid for the herpes simplex virus thymidine kinase gene. *Proc. Natl Acad. Sci. USA* **97**, 354–359 (2000).
128. Heller, L. C. & Heller, R. *In vivo* electroporation for gene therapy. *Hum. Gene Ther.* **17**, 890–897 (2006).
129. Scherer, F. *et al.* Magnetofection: enhancing and targeting gene delivery by magnetic force *in vitro* and *in vivo*. *Gene Ther.* **9**, 102–109 (2002).
130. Manome, Y., Nakamura, M., Ohno, T. & Furuhashi, H. Ultrasound facilitates transduction of naked plasmid DNA into colon carcinoma cells *in vitro* and *in vivo*. *Hum. Gene Ther.* **11**, 1521–1528 (2000).
131. Zintchenko, A., Ogris, M. & Wagner, E. Temperature dependent gene expression induced by PNIPAM-based copolymers: potential of hyperthermia in gene transfer. *Bioconjug. Chem.* **17**, 766–772 (2006).
132. Kloeckner, J., Prasmickaite, L., Hogset, A., Berg, K. & Wagner, E. Photochemically enhanced gene delivery of EGF receptor-targeted DNA polyplexes. *J. Drug Target.* **12**, 205–213 (2004).
133. Lu, J. *et al.* Mesoporous silica nanoparticles for cancer therapy: energy-dependent cellular uptake and delivery of paclitaxel to cancer cells. *Nanobiotechnology* **3**, 89–95 (2007).
134. Tanaka, T. *et al.* Sustained small interfering RNA delivery by mesoporous silicon particles. *Cancer Res.* **70**, 3687–3696 (2010).
135. Lei, C. *et al.* Local release of highly loaded antibodies from functionalized nanoporous support for cancer immunotherapy. *J. Am. Chem. Soc.* **132**, 6906–6907 (2010).
136. Ruoslahti, E., Bhatia, S. N. & Sailor, M. J. Targeting of drugs and nanoparticles to tumors. *J. Cell Biol.* **188**, 759–768 (2010).
137. Hood, J. D. *et al.* Tumor regression by targeted gene delivery to the neovasculature. *Science* **296**, 2404–2407 (2002).
138. Murphy, E. A. *et al.* Nanoparticle-mediated drug delivery to tumor vasculature suppresses metastasis. *Proc. Natl Acad. Sci. USA* **105**, 9343–9348 (2008).
139. Sugahara, K. N. *et al.* Tissue-penetrating delivery of compounds and nanoparticles into tumors. *Cancer Cell* **16**, 510–520 (2009).
140. Pirolo, K. F. & Chang, E. H. Does a targeting ligand influence nanoparticle tumor localization or uptake? *Trends Biotechnol.* **26**, 552–558 (2008).
141. Karmali, P. P. *et al.* Targeting of albumin-embedded paclitaxel nanoparticles to tumors. *Nanomedicine* **5**, 73–82 (2009).
142. Jain, R. K. Delivery of molecular and cellular medicine to solid tumors. *Adv. Drug Deliv. Rev.* **46**, 149–168 (2001).
143. Jain, R. K. Taming vessels to treat cancer. *Sci. Am.* **298**, 56–63 (2008).
144. Northfelt, D. W. *et al.* Pegylated-liposomal doxorubicin versus doxorubicin, bleomycin, and vincristine in the treatment of AIDS-related Kaposi's sarcoma: results of a randomized phase III clinical trial. *J. Clin. Oncol.* **16**, 2445–2451 (1998).
145. O'Brien, M. E. *et al.* Reduced cardiotoxicity and comparable efficacy in a phase III trial of pegylated liposomal doxorubicin HCl (CAELYX/Doxil) versus conventional doxorubicin for first-line treatment of metastatic breast cancer. *Ann. Oncol.* **15**, 440–449 (2004).
146. Gill, P. S. *et al.* Randomized phase III trial of liposomal daunorubicin versus doxorubicin, bleomycin, and vincristine in AIDS-related Kaposi's sarcoma. *J. Clin. Oncol.* **14**, 2353–2364 (1996).
147. Lee, K. S. *et al.* Multicenter phase II trial of Genexol-PM, a Cremophor-free, polymeric micelle formulation of paclitaxel, in patients with metastatic breast cancer. *Breast Cancer Res. Treat.* **108**, 241–250 (2008).
148. Kim, J. & Shin, S. Cost-effectiveness of Genexol-PM for treating metastatic breast cancer. *J. Breast Cancer* **13**, 104–110 (2010).
149. Sevick, E. M. & Jain, R. K. Blood flow and venous pH of tissue-isolated Walker 256 carcinoma during hyperglycemia. *Cancer Res.* **48**, 1201–1207 (1988).
150. Sevick, E. M. & Jain, R. K. Geometric resistance to blood flow in solid tumors perfused *ex vivo*: effects of tumor size and perfusion pressure. *Cancer Res.* **49**, 3506–3512 (1989).
151. Sevick, E. M. & Jain, R. K. Viscous resistance to blood flow in solid tumors: effect of hematocrit on intratumor blood viscosity. *Cancer Res.* **49**, 3513–3519 (1989).
152. Less, J. R., Skalak, T. C., Sevick, E. M. & Jain, R. K. Microvascular architecture in a mammary carcinoma: branching patterns and vessel dimensions. *Cancer Res.* **51**, 265–273 (1991).
153. Baish, J. W. & Jain, R. K. Fractals and cancer. *Cancer Res.* **60**, 3683–3688 (2000).
154. Less, J. R., Posner, M. C., Skalak, T. C., Wolmark, N. & Jain, R. K. Geometric resistance and microvascular network architecture of human colorectal carcinoma. *Microcirculation* **4**, 25–33 (1997).
155. Sun, C., Jain, R. K. & Munn, L. L. Non-uniform plasma leakage affects local hematocrit and blood flow: implications for inflammation and tumor perfusion. *Ann. Biomed. Eng.* **35**, 2121–2129 (2007).

#### Acknowledgments

We thank L. Munn, Y. Boucher, S. Goel, V. Chahaun and B. Diop-Frimpong for their helpful comments on the manuscript. This work was supported by the National Institutes of Health (P01-CA80124, R01-CA126642, R01-CA115767, R01-CA85140, T32-CA73479), a Federal Share Income Grant, and a DoD Breast Cancer Research Innovator award (BC095991). T. Stylianopoulos was supported by a post-doctoral research fellowship from the Susan G. Komen Breast Cancer Foundation (KG091281).

#### Author contributions

R. K. Jain and T. Stylianopoulos both contributed to researching data for the article, discussion of content and writing and editing the manuscript.